RSC Advances

PAPER

View Article Online
View Journal | View Issue

Cite this: *RSC Adv.*, 2020, **10**, 8027

Ameliorative effect of urolithin A on D-gal-induced liver and kidney damage in aging mice *via* its antioxidative, anti-inflammatory and antiapoptotic properties

Peng Chen, †[a] Jiexin Lei,†[b] Fuchao Chen[c] and Benhong Zhou *[a]

Urolithin A, a metabolite produced by human colon microflora from ellagic acid and related compounds, has been reported to have antioxidant, anti-inflammatory and antiapoptotic properties. The present study investigates the protective effects of urolithin A (Uro A) on D-galactose (D-gal)-induced liver and kidney injury and the possible mechanisms in mice. In this study, we first investigated the antioxidant ability of Uro A *in vitro*. Then mice were treated with D-gal subcutaneously (150 mg kg^{-1} d^{-1}), followed by Uro A at different dosages (50, 100, 150 mg kg^{-1} d^{-1}, administered orally) for 8 weeks. The levels of aspartate aminotransferase (AST), alanine aminotransferase (ALT), blood urea nitrogen (BUN) and creatinine (Cr) in the serum were tested. Histopathological features were assessed by hematoxylin and eosin (HE) staining followed by an assessment of the antioxidant and anti-inflammatory activities. Furthermore, we also evaluated the expression levels of the genes Bax, Bcl-2 and cleaved caspase-3 in the liver and kidney. The results showed that Uro A treatment obviously attenuated D-gal-induced liver and kidney damage. The beneficial effects of Uro A were accompanied by a decline in malondialdehyde (MDA) levels and a rise in the superoxide dismutase (SOD), glutathione peroxidase (GSH-Px), catalase (CAT), and total antioxidant capacity (T-AOC) activity in the liver and kidney and downregulation of the levels of inflammatory cytokines, such as tumor necrosis factor-α (TNF-α), interleukin-1 beta (IL-1β) and interleukin-6 (IL-6), in serum. Moreover, Uro A could modulate the expression of Bax, Bcl-2 and cleaved caspase-3 in the livers and kidneys of aging mice. These findings suggested that Uro A ameliorated D-gal-induced liver and kidney injury through attenuating oxidative stress, inflammatory responses and apoptosis.

Received 25th January 2020
Accepted 16th February 2020

DOI: 10.1039/d0ra00774a

rsc.li/rsc-advances

Introduction

Aging is a gradual and biological process that has received great attention and interest from society.[1] Accumulating evidence has shown that aging is one of the greatest risk factors leading to the dysfunction of normal cellular modulation, and aging is associated with numerous diseases, including diabetes, cancers, cardiovascular and cerebrovascular diseases (CCD), Alzheimer's disease (AD) and others, which are harmful to the health of aged people.[2,3] Thus, anti-aging has become one of the hot research topics with an increasing elderly population worldwide.

The free radical theory of aging posits that oxidative stress and reactive oxygen species (ROS) accumulation-induced cell and tissue damage play a critical role in the pathological process of aging.[4] Plenty of evidence has demonstrated that oxygen free radicals, which are generated during metabolism and energy production in the body, are closely related to the regulation of signal transduction and gene expression as well as redox homeostasis.[5] However, high levels of ROS can cause the peroxidation of membrane lipids, and damage to DNA, proteins and phospholipids, eventually resulting in cellular injury, apoptosis and inflammation.[6] Furthermore, natural antioxidants have been proven to be successful scavengers of oxygen radicals, which can prevent the peroxidation of lipids and delay aging.

It has been confirmed that chronic injections of D-galactose (D-gal) can simulate the pathology of aging along with liver and kidney injury.[7] D-gal is a normal reducing sugar in the body that can be metabolized into glucose at normal levels; however, D-gal can be converted into aldose and hydroperoxides under the action of oxidase at high concentrations, leading to the formation of the superoxide anion and oxygen-derived free radicals that can form advanced glycation end products (AGEs) *in vivo*.[8] Evidence has shown that excessive AGEs can accelerate the

[a]*Department of Pharmacy, Renmin Hospital of Wuhan University, Wuhan, Hubei, 430060, P. R. China. E-mail: benhongzh@whu.edu.cn; Tel: +86 15335898431*
[b]*Department of Endocrinology, Renmin Hospital of Wuhan University, Wuhan, Hubei, 430060, P. R. China*
[c]*Department of Pharmacy, Dongfeng Hospital, Hubei University of Medicine, Shiyan, Hubei, 442008, P. R. China*
† These authors contributed equally to this work.

production of intracellular ROS and result in the accumulation of oxidative stress. The liver and kidney are vulnerable to D-gal-induced oxidative damage, which could lead to an increase in ROS generation, a decline in antioxidant enzyme content and the inflammatory response.[9,10] Therefore, systemic administration of D-gal could be applied to establish an animal aging model for an organ damage study.

Urolithin A ($C_{13}H_8O_4$, 3,8-dihydroxy-6*H*-benzo[*c*]chromen-6-one, Uro A; the chemical structure is shown in Fig. 1A), also named 3,8-dihydroxy-urolithin, is a type of microflora human metabolite that is produced by the gut microbiota from ellagitannins (ETs) and ellagic acid (EA) and has been reported to possess a high capacity to scavenge free radicals.[11] Furthermore, abundant *in vivo* research has indicated that urolithin A possesses a variety of pharmacological activities, such as antioxidative, anti-inflammatory, and antiapoptotic effects.[12,13] Because of its great antioxidant activity, urolithin A may play a vital role in protecting against these oxidative stress-mediated pathological conditions.[14] Recently, the anti-aging effects of urolithin A have drawn considerable attention, and it has been confirmed that urolithin A can induce mitophagy, prolong the lifespan of *C. elegans* and increase muscle function in rodents.[15] However, there are still no scientific reports to date on the protective effects of urolithin A on D-gal-induced aging and D-gal-induced liver and kidney injury.

Thus, the present study was performed to investigate how urolithin A ameliorates D-gal-caused liver and kidney injury and to explore the potential underlying mechanisms, which will provide a comprehensive foundation for the theoretical basis and practical application of urolithin A in the prevention or treatment of aging-associated diseases.[16]

Materials and methods

Materials

D-gal (cat. no. T9420, purity >99%) was purchased from Guangyuan Hengxin Technology Development Co., Ltd. (Beijing, China). The urolithin A standard was purchased from Sigma Chemical Co. (St. Louis, MO, USA, cat. no. 100151-231, purity >99%). Malondialdehyde (MDA, cat. no. A003-2), superoxide dismutase (SOD, cat. no. A043-1), glutathione (GSH, cat. no. A037-2), catalase (CAT, cat. no. A023-4) enzyme, total antioxidant capacity (T-AOC, cat. no. A028-5), aspartate aminotransferase (AST, cat. no. A045-2), alanine aminotransferase (ALT, cat. no. A024-6), blood urea nitrogen (BUN, cat. no. A048-1) and creatinine (Cr, cat. no. A037-4) assay kits were purchased from Nanjing Jiancheng Biotechnology Co., Ltd. (Nanjing, China). ELISA assay kits for tumor necrosis factor-α (TNF-α, cat. no. sc-1462), interleukin-1 beta (IL-1β, cat. no. sc-1457) and interleukin-6 (IL-6, cat. no. sc-1471) were obtained from Santa Cruz Biotechnology, Inc. (Santa Cruz, CA, USA). Antibodies against Bax (cat. no. MA5-14003), Bcl-2 (cat. no. MA5-11757) and cleaved caspase-3 (cat. no. PA5-23921) were obtained from Thermo Fisher Scientific (Shanghai, China). β-Actin (1 : 1000; cat. no. 48727) and goat anti-rabbit IgG antibodies (1 : 30 000; cat. no. sc-2005) were acquired from Santa Cruz Biotechnology, Inc. (Santa Cruz, CA, USA). All other solvents and chemicals used in the experiments were of at least analytical grade and purity.

In vitro antioxidant activities

DPPH radical scavenging assay. The assessment of DPPH radical scavenging capacity of urolithin A was performed according to the previous method with only minor modifications.[12] Urolithin A were dissolved by 50% ethanol and diluted into a gradient solution of 30–200 μg mL^{-1} samples. Then 2 mL of sample solution was mixed with 2 mL of 0.24 mM DPPH solution in 95% ethanol, and the mixtures were fully shaken and placed in the dark place for 30 min at room temperature. After that, the absorbance (Abs) of mixtures was measured at 519 nm with UV visible spectrophotometry. Vitamin C (VC) was used for the positive control in this study. The DPPH radical scavenging activity (%) was defined as follows: scavenging rate (%) = $(A_{Control} - A_{Sample})/A_{Control} \times 100\%$.

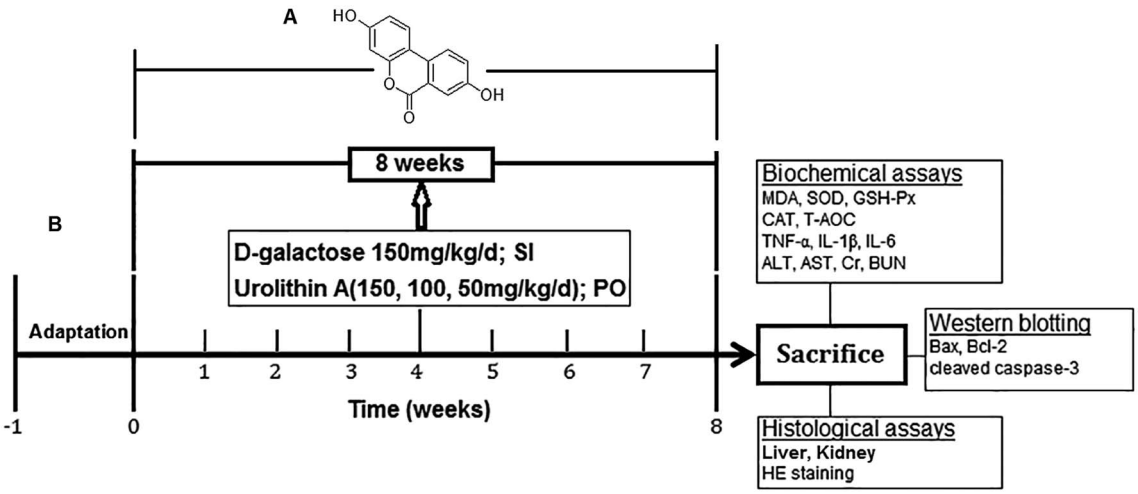

Fig. 1 (A) Molecular structure of urolithin A. (B) Schematic representation of treatment schedule followed for the modulation of aging using D-gal and urolithin A. SI: Subcutaneous Injection; PO: Per Oral.

$ABTS^+$ radical scavenging assay. The $ABTS^+$ radical scavenging activities of urolithin A was determined based on a published report.[13] In brief, the isometric 7.4 mM $ABTS^+$ aqueous solution and 2.6 mM $K_2S_2O_8$ aqueous solution were mixed and placed for overnight to prepare for $ABTS^+$ stock solution. The $ABTS^+$ stock solution was diluted 1 : 40 (*v*/*v*) using 95% ethanol to obtain proper absorbance of 0.7 ± 0.02 at a wavelength of 734 nm. Then 1.2 mL $ABTS^+$ diluent was mixed with 0.3 mL of urolithin A solution varied from 30 to 200 μg mL^{-1}, and incubated at room temperature for 5 min, after which the absorbance was detected at 734 nm. The calculation formula of scavenging rate (%) was $[(A_{Control} - A_{Sample})/A_{Control}] \times 100\%$. VC was used as a positive control in this study. Each sample was measured in quintuplicate.

Superoxide anion radical scavenging. The superoxide anion radical assay was determined as described previously.[14] Urolithin A solution was prepared by mixing 1 mL of 30–200 μg mL^{-1} urolithin A with 3 mL of Tris–HCl buffer (pH = 8.2), and then 100 μL pyrogallol was added and mixed well. After 2 minutes, the absorbance was recorded at 325 nm every 30 s for 5 minutes using a spectrophotometer. The ability to scavenge $O_2^{-\cdot}$ radicals was expressed as $[(A_{Control} - A_{Sample})/A_{Control}] \times 100\%$.

OH^- scavenging activity assay. OH^- scavenging activity assay was performed following the method of Smirnoff and Cumbes.[15,16] The reaction mixture contained 1 mL $FeSO_4$ (9 mM), 1 mL H_2O_2 (9 mM), 1 mL of various concentrations extract solution and 1 mL ethanol with 9 mM salicylic acid. The total mixture was incubated at 35 °C for 30 min, and then the absorbance was read at 510 nm. Ascorbic acid was used as the positive control. OH^- scavenging activity was calculated by the following equation: scavenging rate (%) = $[(\Delta A_{Control}/T - \Delta A_{Sample}/T)/(\Delta A_{Control}/T) \times 100\%$, $T = 5$ min].

Animal study *in vivo*

Sixty adult male Institute of Cancer Research (ICR) mice (4 weeks old, weighing 19.9–27.5 g) were purchased from Wuhan Institute of Biological Products Co. (Wuhan, China). All groups of animals were kept at a regulated temperature (22 ± 2 °C) and humidity (50 ± 10%) on a 12 hour light/dark cycle with *ad libitum* access to standard commercial food and pure water. All procedures were approved by the internal ethical committee of Wuhan University (IACUCWU protocol number: SCXK (E) 2013-0004).

After one week of adaptive feeding, the mice were randomized into 5 groups ($n = 12$ per group): normal control group, aging model group (D-gal, 150 mg kg^{-1} d^{-1}), D-gal (150 mg kg^{-1} d^{-1}) + urolithin A (150 mg kg^{-1} d^{-1}) group, D-gal (150 mg kg^{-1} d^{-1}) + urolithin A (100 mg kg^{-1} d^{-1}) group and D-gal (150 mg kg^{-1} d^{-1}) + urolithin A (50 mg kg^{-1} d^{-1}) group. Except for the normal control group, all groups were administered D-gal (150 mg kg^{-1} d^{-1} for 8 weeks) daily *via* subcutaneous injection (SI), which was dissolved in 0.9% normal saline (NS); the control group was subjected to 0.9% NS injection in the same way. Then, mice in the urolithin A groups were administered with urolithin A (150, 100, 50 mg kg^{-1} d^{-1}), dissolved in 0.5% carmellose sodium (CMC-Na) *via* gavage for 8 consecutive weeks, while the mice in the control group and model group were subjected to equal volumes of 0.5% CMC-Na in the same way.[17,18] All mice were fed a standard pellet diet, and water was freely available (the experimental design is illustrated in Fig. 1B). The dose of urolithin A used in the present study was according to a preliminary experiment in our lab. The body weight of the mice was measured every 3 days using electronic scale during the experiment. And we observed the hair color and mental state of mice with the naked eye and then recorded them before and after the experiment. The animal experiments were carried out in accordance with the guidelines of ARRIVE (Animal Research: Reporting *In Vivo* Experiments).

Tissue preparation

At the end of the treatment period, the mice were anesthetized intraperitoneally with a ketamine–xylazine mixture (100 mg kg^{-1} and 10 mg kg^{-1}, respectively). Following decapitation, 0.1 mL blood samples were collected with the addition of anticoagulants for centrifugation at 3000 × *g* for 10 min for the subsequent determination of clear serum, the liver and kidney from each animal were rapidly removed, and the organ tissues were quickly dissected on ice, rinsed with saline, and frozen at −80 °C until use. The frozen tissues were thawed and homogenized in cold PBS at a pH of 7.4 (100 mg tissue per 1 mL of the buffer), which contained a protease inhibitor cocktail.[6] The samples were centrifuged at 10 000 × *g* for 20 min at 4 °C, and the clear supernatants were collected carefully, divided into aliquots, and stored immediately at −80 °C until analysis.[7] The total protein concentration of each supernatant was determined using a Bio-Rad protein assay kit according to the manufacturer's protocol. In addition, we weighed the livers and kidneys for the organ coefficient calculation (ratio of organ weight to body weight).

Hematoxylin and eosin (HE) staining

For histomorphological examinations, all samples were fixed in 4% formaldehyde buffer followed by embedding in paraffin and slicing longitudinally, with 5 μm-thick sections obtained for hematoxylin–eosin staining for histomorphological analysis.[4,5] Furthermore, liver and kidney histopathological score was performed. Briefly, the degree of necrosis in liver was expressed as the mean of twelve different fields within each classified on a scale of 0–3 (normal-0, mid-1, moderate-2, severe-3). The number of inflammatory cells was counted in twelve randomly selected fields from each slide at a magnification of 200×. For histological evaluation on kidney, the following parameters were graded on a scale 0–2 (0-absent, 1-mild-moderate, 2-severe): tubular dilatation, lymphocyte infiltration, macrophage infiltration, and dilatation of the Bowman's capsule.

Biochemical analysis

The levels of MDA and protein content, as well as the activities of T-SOD, T-AOC, GSH-Px, and CAT in the liver and kidney tissue were measured using commercially available assay kits. The activities of TNF-α, IL-1β and IL-6 were determined in the liver and kidney tissue supernatant using a standard ELISA kit. All biochemical analyses followed the manufacturer's protocols.

Similarly, the ALT, AST, Cr and BUN concentrations in the serum samples were analyzed with ELISA kits.

Real-time-polymerase chain reaction (RT-PCR)

Total RNA was purified from fresh mouse liver tissue (50–100 mg) on ice with RNA fast 1000. The purity of the total RNA was checked with a spectrophotometer and the wavelength absorption ratio (260/280 nm) was between 1.7 and 2.0 in all preparations. Reverse transcription of total RNA (0.1–5 μg) to cDNA was performed using Revert Aid First Strand cDNA Synthesis Kits in 20 μL reaction volumes at 44 °C for 1 h using a Mastercycler personal PCR machine (Eppendorf AG, Hamburg, Germany). Specific primers were designed using the Beacon Designer 4.0 software and synthesized by Sunbiotech (Beijing Sunbiotech CO., Ltd, China). Real-time PCR was performed with Maxima SYBR Green/ROX qPCR Master Mix (2×) in an IQ 5.0 system. The system automatically monitors the binding of the fluorescent dye SYBR® Green to double-stranded DNA during each cycle of PCR amplification. PCR was performed under the following conditions: (1) heating at 50 °C for 2 min; (2) followed by 95 °C for 10 min and (3) 40 PCR cycles at 94 °C for 15 s, 60 °C for 30 s, and 72 °C for 30 s. The relative amount of mRNA was calculated using the comparative C_t ($\Delta\Delta C_t$) equation. The β-actin gene was used as a reference for normalizing the data. The derived normalized values are the mean of three runs. The mouse and human primer sequences are listed in Table 1.

Western blotting

To determine the protein expression levels of Bax, Bcl-2 and cleaved caspase-3, whole liver and kidney tissues were homogenized at 4 °C in homogenizing buffer (50 mM Tris–Cl pH 7.5), containing 2 mM dithiothreitol (DTT), 2 mM ethylenediaminetetraacetic acid (EDTA), 2 mM ethylene glycol tetraacetate (EGTA), 5 mg mL^{-1} each of leupeptin, aprotinin, pepstatin A, and chymostatin, 50 mM potassium fluoride (KF), 50 nM okadaic acid, 5 mM sodium pyrophosphate, and 2% sodium dodecyl sulfate (SDS). The homogenate was then sonicated to dissolve the tissue completely, and the protein quantities of each sample were determined by a BCA protein assay kit. Equal amounts of protein (100 μg) were isolated by 10% SDS-polyacrylamide gel electrophoresis and were electrophoretically transferred to a nitrocellulose membrane. The membrane was blocked with 5% skim milk powder in a washing buffer [Tris-buffered saline containing 0.05% (*v*/*v*) Tween 20] for 2 h at 25 °C and was incubated with primary rabbit polyclonal antibodies against Bax, Bcl-2 and cleaved caspase-3 at a 1 : 500 dilution at 4 °C overnight. Each membrane was rinsed three times for 15 min each time and incubated with the secondary horseradish peroxidase-linked antibodies. β-Actin was used as an internal control for the cytosolic extracts. Finally, enhanced chemiluminescence (ECL) was adopted to color the brands, and pictures of the proteins were taken and processed with Image-Pro Plus 6.0 software.

Table 1 Real-time PCR primer sequences

Gene	Primer sequence	Product size (bp)
TNF-α	F: 5′-TGTAGCCCACGTCGTAGCAA-3′ R: 5′-ATAGCAAATCGGCTGACGGT-3′	216
IL-1β	F: 5′-TGCCACCTTTTGACAGTGATG-3′ R: 5′-AAGGTCCACGGGAAAGACAC-3′	220
IL-6	F: 5′-CCCCAATTTCCAATGCTCTCC-3′ R: 5′-CGCACTAGGTTTGCCGAGTA-3′	141
β-Actin	F: 5′-TGAGAGGGAAATCGTGCGTG-3′	192

Statistical analysis

Data are expressed as the mean ± standard deviation (SD). The data were analyzed with SPSS 16.0 (SPSS Inc., Chicago, Ill., USA). The statistical significance of the differences in the dependent measures between the experimental groups was determined by one-way ANOVA followed by Tukey's tests. Probability values of less than 0.05 were considered significant. Each experiment was performed at least 3 times.

Results

The antioxidant activity of urolithin A *in vitro*

Oxidative stress (OS), which is a negative effect produced by reactive oxygen species (ROS), has been regarded as one of the most significant factors in the ontogeny of many multifactorial diseases, including aging, cancer, Parkinson's disease and diabetes. DPPH, $ABTS^+$, $O_2^{\cdot}$ and ·OH are four kinds of free radicals that are usually used to assess the antioxidant capacity of natural crude drugs and health foods. Hence, DPPH, $ABTS^+$, $O_2^{\cdot}$·and ·OH assays were evaluated to assess the antioxidant capacity of urolithin A in this study. The results showed that urolithin A possessed a good ability to scavenge DPPH radicals in a dose-dependent manner, and the 50% effective concentration (EC_{50}) (328.21 ± 3.44 μmol L^{-1}) was lower than that of VC (573.13 ± 4.49 μmol L^{-1}) (Fig. 2A). The results from the $ABTS^+$ radical scavenging assay (Fig. 2B) also showed that urolithin A exerted a strong activity to scavenge $ABTS^+$, and it was found that the EC_{50} of urolithin A against $ABTS^+$ was 302.18 ± 2.67 μmol L^{-1}, whereas that of VC was 487.72 ± 4.07 μmol L^{-1}. The scavenging effects of urolithin A on $O_2^{\cdot}$ and ·OH were also determined, and the results showed that the EC_{50} of urolithin A and VC for $O_2^{\cdot}$(·OH) were 333.12 ± 5.42 (504.54 ± 4.71) μmol L^{-1} and 523.476 ± 3.67 (916.58 ± 5.29) μmol L^{-1}, respectively, indicating that the scavenging rate of urolithin A towards $O_2^{\cdot}$ and ·OH was comparable to VC (Fig. 2C and D).

Effect of urolithin A on D-gal induced liver and kidney damage *in vivo*

Effect of urolithin A on the general appearance, body weight and organ indexes. The control group was active, sensitive to sound and light, possessed white and shiny hair with no depression or drowsiness from the 6th week. Compared with the control group, the mice in the model group were dull, unresponsive, and their hair was lusterless. However, these deterioration symptoms alternated in the mice in the urolithin A groups. All animals in our study showed no concerning signs

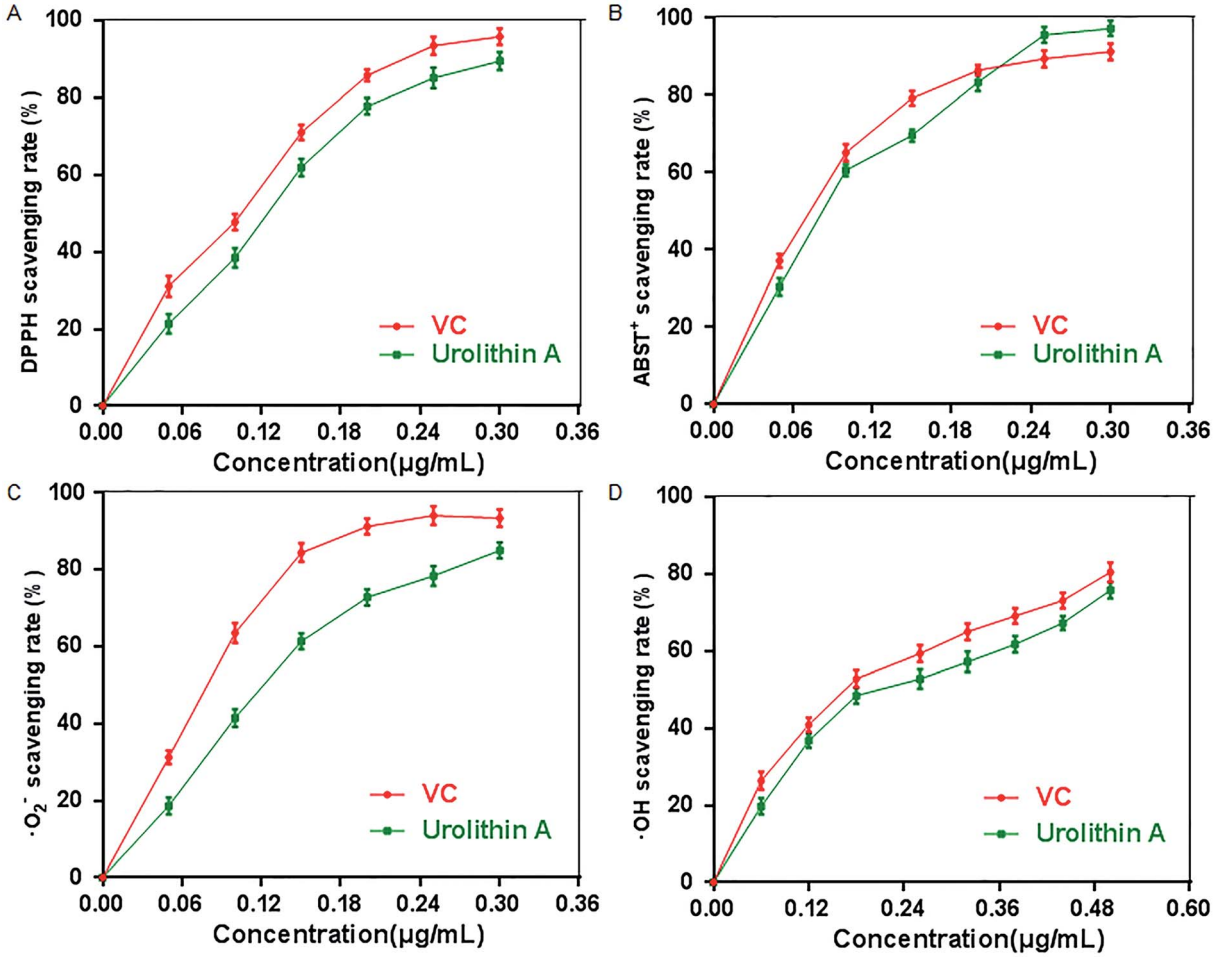

Fig. 2 Effect of urolithin A on antioxidant activity *in vitro*. (A) DPPH scavenging assay. (B) $ABTS^+$ scavenging assay. (C) $O_2^{\bullet}$ scavenging assay. (D) ·OH scavenging assay. The data are expressed as means ± SD ($n = 5$).

leading to the early termination/sacrifice of that animal during the experiment. Moreover, after 8 weeks of D-gal injection, compared with the control group, there was a significant decrease in the body weight and liver/kidney index in the model group induced by D-gal ($P < 0.05$ or $P < 0.01$), but these decreases could be attenuated after the intervention with urolithin A compared to the aging group mice ($P < 0.05$ or $P < 0.01$, Table 2).

Effect of urolithin A on the MDA content and SOD, GSH-Px, CAT, and T-AOC activities in liver and kidney. The MDA level in the model group significantly increased compared with the control group. The administration of urolithin A (150, 100 and 50 mg kg^{-1}) resulted in a decline in the MDA level compared with the D-gal alone treated mice (all $P < 0.05$ or $P < 0.01$, Fig. 3C). In addition, the activities of SOD, GSH-Px, CAT, and T-AOC in the liver and kidney of the model mice were found to be significantly decreased compared with the control group (all $P < 0.05$ or $P < 0.01$), and urolithin A (150, 100 and 50 mg kg^{-1}) could significantly improve these biochemical indices, which

Table 2 Effect of urolithin A on body weight and organ coefficients after the 8 week experimental period. Data are presented as mean ± SD from each group ($n = 12$, mean ± SD). $^{\#}P < 0.05$ and $^{\#\#}P < 0.01$ *vs.* control group; $^{*}P < 0.05$ and $^{**}P < 0.01$ *vs.* model group

		Organ index (mg g^{-1})	
Groups	Body weight (g)	Liver	Kidney
Control	44.95 ± 1.02	10.82 ± 0.47	5.72 ± 0.38
D-gal (150 mg kg^{-1})	39.68 ± 0.95$^{\#\#}$	7.98 ± 1.23$^{\#\#}$	4.45 ± 0.29$^{\#\#}$
D-gal + Uro A (150 mg kg^{-1})	44.56 ± 1.12**	9.97 ± 0.86**	5.60 ± 0.18**
D-gal + Uro A (100 mg kg^{-1})	43.78 ± 1.34**	9.84 ± 0.73**	5.12 ± 0.61**
D-gal + Uro A (50 mg kg^{-1})	42.47 ± 0.96**	8.79 ± 0.42*	5.03 ± 0.24*

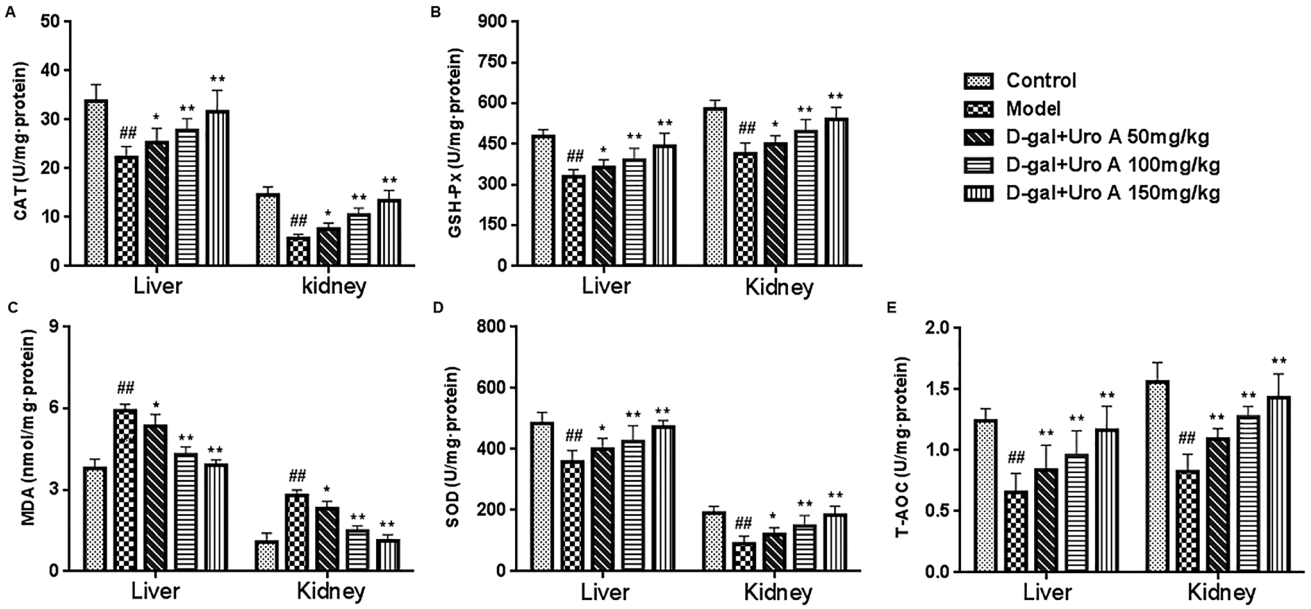

Fig. 3 Effect of urolithin A on CAT (A), GSH-Px (B), MDA (C), SOD (D), and T-AOC (E) in liver and kidney. Data are presented as mean ± SD from each group ($n = 12$, mean ± SD). $^{\#}P < 0.05$ and $^{\#\#}P < 0.01$ *vs.* control group; $^{*}P < 0.05$ and $^{**}P < 0.01$ *vs.* model group.

was significantly different from the model group (all $P < 0.05$ or $P < 0.01$, Fig. 3A, B, D and E). Overall, these results indicated that urolithin A exerted antioxidant effects in the livers and kidneys of D-gal-induced aging mice.

Effect of urolithin A on the activity of TNF-α, IL-1β and IL-6 in liver and kidney. As illustrated in Fig. 4, the levels of TNF-α, IL-6 and IL-1β in the livers and kidneys of the D-gal-induced aging model mice were significantly increased compared to the control group mice (all $P < 0.05$ or $P < 0.01$, Fig. 4A–C). Furthermore, after treatment with urolithin A, the activities of TNF-α, IL-6 and IL-1β in the liver and kidney were significantly upregulated (all $P < 0.01$, Fig. 4).

As seen from Fig. 5, our result showed that the mRNA levels of TNF-α, IL-6 and IL-1β in the livers and kidneys in model group was significantly higher than that of control group (all $P < 0.05$ or $P < 0.01$, Fig. 5A–C). As a result, after supplementation of urolithin A, the mRNA levels of TNF-α, IL-6 and IL-1β could be significantly lowered in livers and kidneys of aging mice induced by D-gal when compared with the model group (all $P < 0.01$, Fig. 5). These findings showed that urolithin A could improve the inflammatory status of aging mice.

Effect of urolithin A on liver and kidney functions. As shown in Fig. 6, ALT and AST levels in the serum significantly increased after treatment with D-gal in aging mice when compared with the control group (both $P < 0.01$). As a result, after urolithin A supplementation (150, 100 and 50 mg kg^{-1}), the levels of ALT and AST were significantly restored in the treatment groups compared to the model group (both $P < 0.01$). These findings showed that urolithin A could improve hepatic function and liver damage.

As presented Fig. 7, D-gal administration resulted in a significant increase in Cr and BUN (both $P < 0.01$) levels compared with the control, which suggests that D-gal may induce renal function decline. However, the increase in the levels of Cr and BUN were significantly inhibited by all three tested doses of urolithin A in our study ($P < 0.05$ or $P < 0.01$). The results suggest that urolithin A may possess a protective effect against D-gal-induced renal dysfunction.

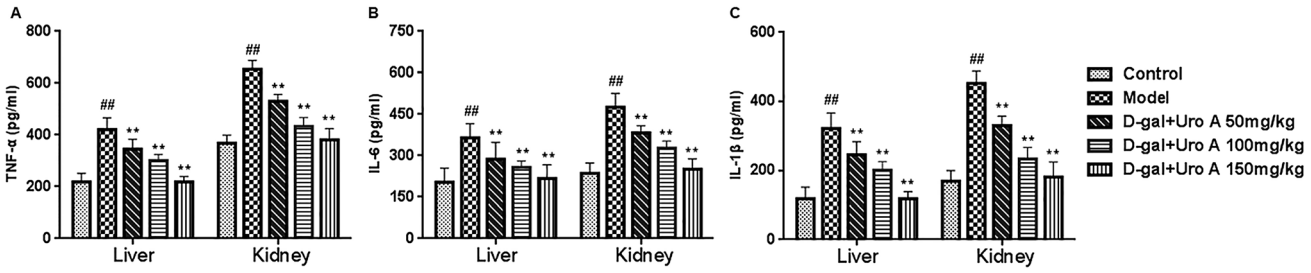

Fig. 4 Effect of urolithin A on the TNF-α (A), IL-1β (B) and IL-6 (C) level in serum of mice. The levels of TNF-α, IL-1β and IL-6 were quantified using ELISA kits. Data are presented as mean ± SD from each group ($n = 12$, mean ± SD). $^{\#}P < 0.05$ and $^{\#\#}P < 0.01$ *vs.* control group; $^{*}P < 0.05$ and $^{**}P < 0.01$ *vs.* model group.

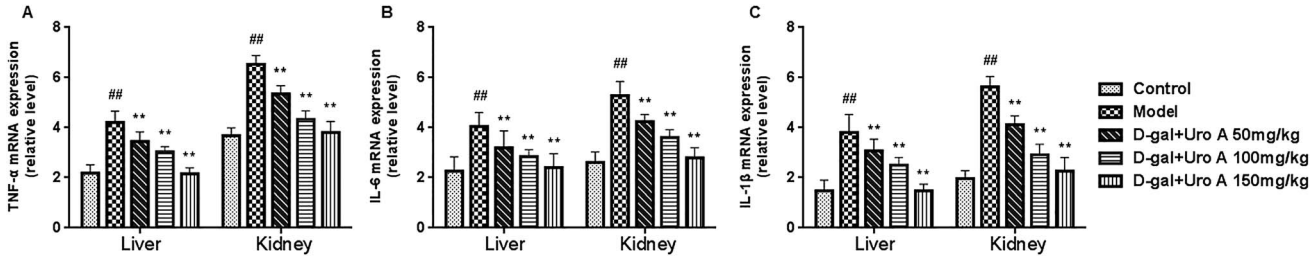

Fig. 5 Effect of urolithin A on the TNF-α (A), IL-1β (B) and IL-6 (C) mRNA expression in serum of mice. The expression of TNF-α, IL-1β and IL-6 in different groups was analyzed through quantitative RT-PCR. Data are presented as mean ± SD from each group ($n = 12$, mean ± SD). $^{\#}P < 0.05$ and $^{\#\#}P < 0.01$ *vs.* control group; $^{*}P < 0.05$ and $^{**}P < 0.01$ *vs.* model group.

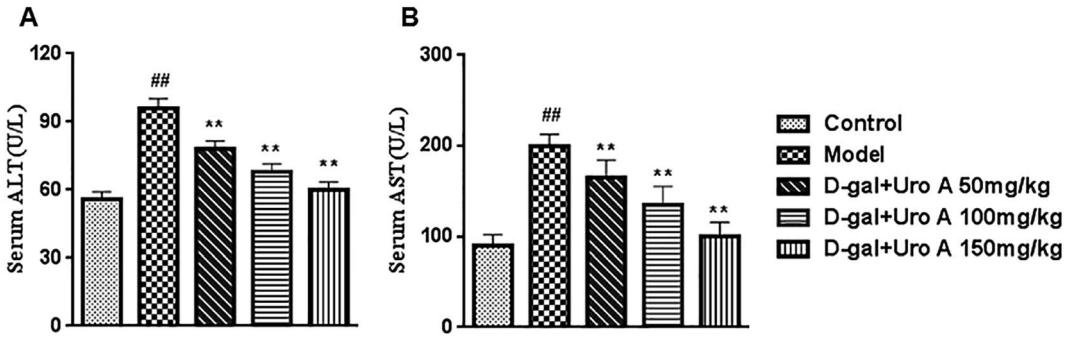

Fig. 6 Effect of urolithin A on AST (A) and ALT (B) activities in serum. Data are presented as mean ± SD from each group ($n = 12$, mean ± SD). $^{\#}P < 0.05$ and $^{\#\#}P < 0.01$ *vs.* control group; $^{*}P < 0.05$ and $^{**}P < 0.01$ *vs.* model group.

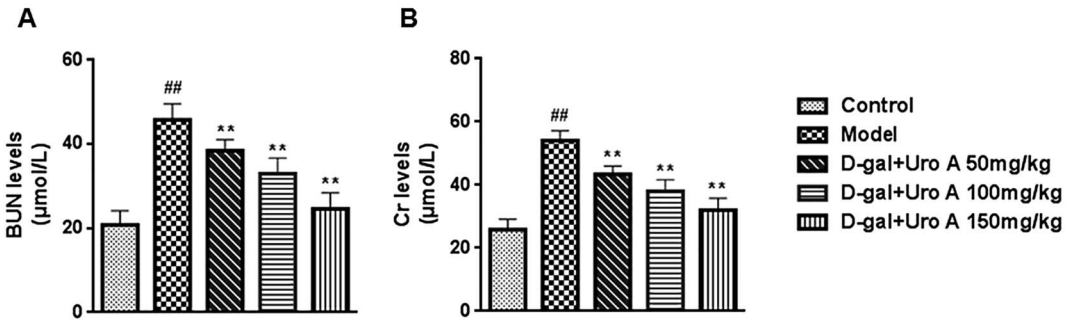

Fig. 7 Effect of urolithin A on BUN (A) and Cr (B) activities in serum. Data are presented as mean ± SD from each group ($n = 12$, mean ± SD). $^{\#}P < 0.05$ and $^{\#\#}P < 0.01$ *vs.* control group; $^{*}P < 0.05$ and $^{**}P < 0.01$ *vs.* model group.

Liver and kidney histomorphology

As shown in Fig. 8, the model group showed significant liver damage, including hepatocellular hydropic degeneration, necrosis, and inflammatory cell infiltration. However, there was an obvious increase in the hepatocellular hydropic degeneration and necrosis upon treatment with urolithin A compared to the mice in the model group. Above all, the morphological structure after urolithin A (150 mg kg^{-1}) treatment appeared very similar to that of the control group. The results of histopathological scores showed that the number of inflammatory cells and necrosis scores in model group mice were much higher than the control group (both $P < 0.01$, Table 3), indicating that there was a significant difference in histopathological change between control and D-gal treated mice ($P < 0.05$ or $P < 0.01$, Table 3). In contrast, urolithin A treatment noticeably ameliorated the spontaneous activity defects ($P < 0.05$ or $P < 0.01$). These findings suggest that hepatic pathological changes could be ameliorated by urolithin A intervention.

As shown in Fig. 9, normal renal histomorphology was found in the control group and without noticeable differences in morphological changes compared to the positive control group. By contrast, D-gal injection led to evident glomerular and tubulointerstitial damage, such as glomerular basement membrane thickening, tubular necrosis, cell apoptosis, in aging mice. However, urolithin A treatment reversed these pathological changes, and the high-dose group of urolithin A (150 mg kg^{-1}) showed the maximal protective effect, with minor changes in morphological structure that were almost identical to the normal

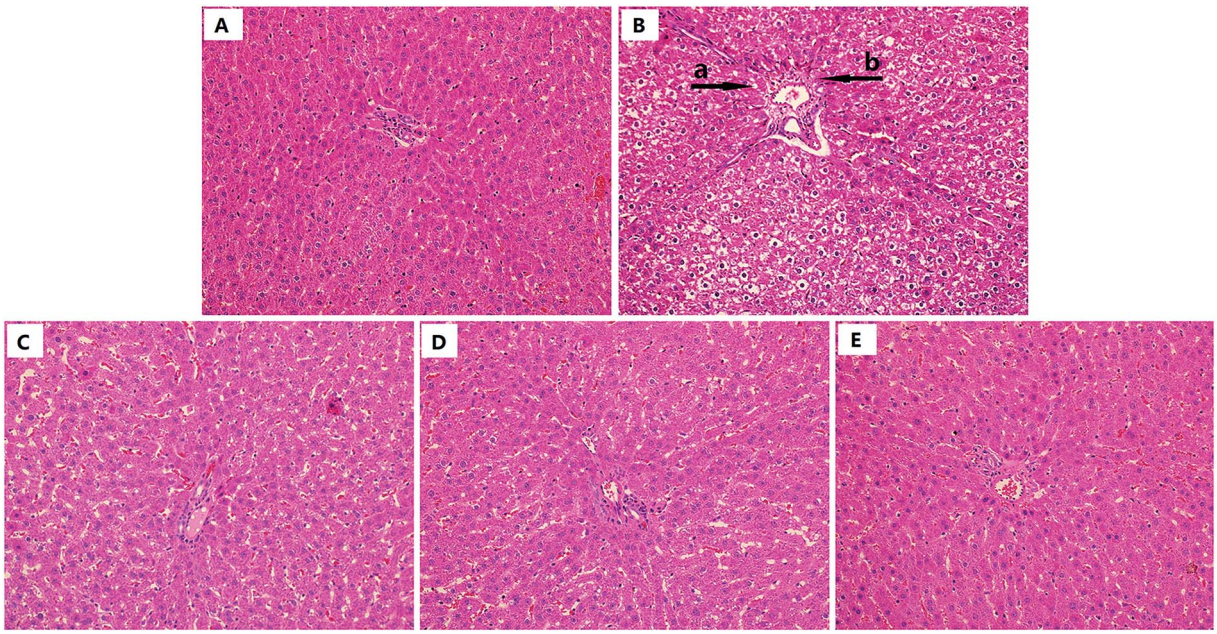

Fig. 8 Effect of urolithin A treatment on liver histopathological alterations. (H&E staining, magnification 200×). (A) Control group; (B) model group; (C) D-gal + urolithin A group (50 mg kg^{-1}); (D) D-gal + urolithin A group (100 mg kg^{-1}); (E) D-gal + urolithin A group (150 mg kg^{-1}). (a arrow indicated inflammatory infiltration; b arrow indicated apoptosis and necrosis)

Table 3 The effects of urolithin A on D-gal-induced liver histopathologic damage in aging mice. Data are presented as mean ± SD from each group (n = 12, mean ± SD). $^{\#}P < 0.05$ and $^{\#\#}P < 0.01$ *vs.* control group; $^{*}P < 0.05$ and $^{**}P < 0.01$ *vs.* model group

Groups	Animals (n)	The number of inflammatory cells (cells per field, mean ± SD)	Necrosis (scale, mean ± SD)
Control	12	71.90 ± 2.1	0 ± 0
D-gal (150 mg kg^{-1})	12	146.21 ± 21.2$^{\#\#}$	1.80 ± 0.16$^{\#\#}$
D-gal + Uro A (150 mg kg^{-1})	12	60.63 ± 4.7**	0.30 ± 0.14**
D-gal + Uro A (100 mg kg^{-1})	12	97.24 ± 3.3**	0.80 ± 0.11**
D-gal + Uro A (50 mg kg^{-1})	12	121.40 ± 14.2*	1.40 ± 0.13*

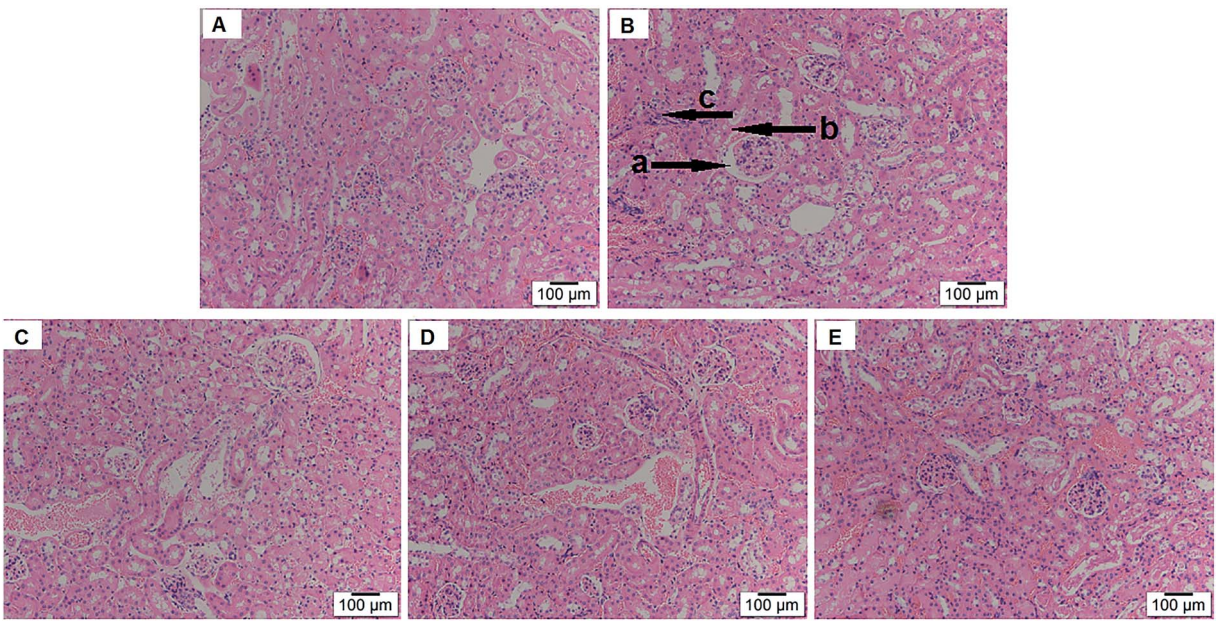

Fig. 9 Effect of urolithin A treatment on kidney histopathological alterations. (H&E staining, magnification 200×). (A) Control group; (B) model group; (C) D-gal + urolithin A group (50 mg kg^{-1}); (D) D-gal + urolithin A group (100 mg kg^{-1}); (E) D-gal + urolithin A group (150 mg kg^{-1}). (a arrow indicated glomerular basement membrane thickening, b arrow indicated tubular necrosis, c arrow indicated apoptosis)

Table 4 The effects of urolithin A on D-gal-induced kidney histopathologic damage in aging mice. Data are presented as mean ± SD from each group (n = 12, mean ± SD). $^{\#}P < 0.05$ and $^{\#\#}P < 0.01$ *vs.* control group; $^{*}P < 0.05$ and $^{**}P < 0.01$ *vs.* model group

Groups	Animals (n)	Tubular dilatation (scale, mean ± SD)	Lymphocyte infiltration (scale, mean ± SD)	Macrophage infiltration (scale, mean ± SD)	Dilatation of the Bowman's capsule (scale, mean ± SD)
Control	12	0.20 ± 0.03	0.31 ± 0.02	0.19 ± 0.08	0.25 ± 0.04
D-gal (150 mg kg^{-1})	12	1.61 ± 0.22$^{\#\#}$	1.73 ± 0.17$^{\#\#}$	1.78 ± 0.14$^{\#\#}$	1.81 ± 0.24$^{\#\#}$
D-gal + Uro A (150 mg kg^{-1})	12	0.30 ± 0.07**	0.41 ± 0.07**	0.33 ± 0.06**	0.43 ± 0.04**
D-gal + Uro A (100 mg kg^{-1})	12	0.84 ± 0.25**	0.87 ± 0.11**	0.92 ± 0.25**	0.94 ± 0.21**
D-gal + Uro A (50 mg kg^{-1})	12	1.20 ± 0.02*	1.26 ± 0.16*	1.30 ± 0.22*	1.35 ± 0.08*

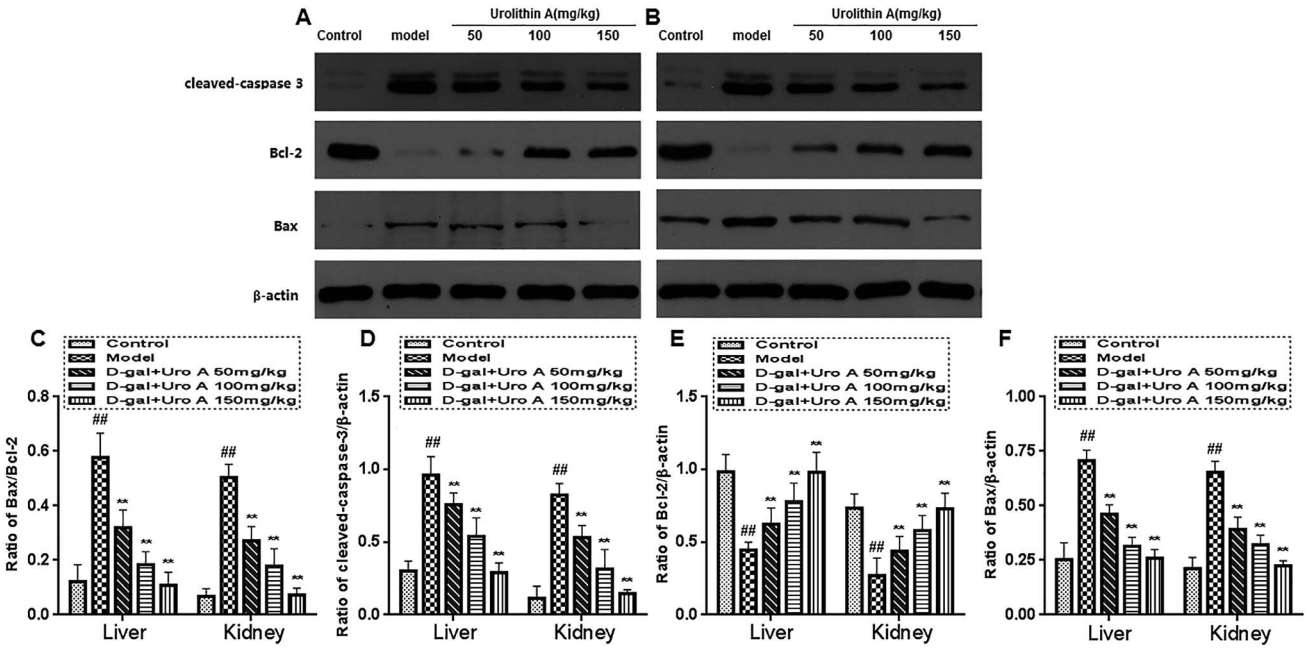

Fig. 10 Effect of urolithin A on the expressions of Bcl-2, Bax and cleaved caspase-3 in liver (A) and kidney (B). Quantification of Bax/Bcl-2 ration (C), cleaved caspase-3/β-actin ratio (D), Bcl-2/β-actin ration (E) and Bax/β-actin ration (F) in liver and kidney. Data are presented as mean ± SD from each group (n = 12, mean ± SD). $^{\#}P < 0.05$ and $^{\#\#}P < 0.01$ *vs.* control group; $^{*}P < 0.05$ and $^{**}P < 0.01$ *vs.* model group.

control group. The histopathological scores results showed that the degree of lymphocyte and macrophage infiltration was greater in model group when compared to control group, reaching a level of statistical significance after D-gal administration, respectively (both $P < 0.01$, Table 4). The degree of tubular dilation as well as that of the Bowman's capsule significantly differed between the control group and aging group (both $P < 0.01$, Table 4). However, these parameters were improved by urolithin A ($P < 0.05$ or $P < 0.01$). These results showed that urolithin A treatment produced a significant effect on the amelioration of the renal injury caused by D-gal.

Western blot analysis

Fig. 10 indicates the effect of urolithin A on the protein expression of Bcl-2, Bax and cleaved caspase-3 during the D-gal-induced aging process. D-gal injection significantly increased the expression level of cleaved caspase-3 and the ratio of Bax/Bcl-2 when compared to the vehicle control (both $P < 0.01$). However, the protein expression of cleaved caspase-3 and the Bax/Bcl-2 ratio were significantly downregulated after 8 weeks of treatment with urolithin A in a concentration-dependent manner (both $P < 0.01$).

Discussion

Aging is a biological process influenced by a variety of complex factors, such as heredity, environmental conditions and life-style. The free radical theory of aging states that oxidative damage caused by reactive oxygen species (ROS) or free radicals induced from cell metabolism is a key factor that accelerates aging.[19] Although the mechanisms of aging are complex and mysterious, many recent studies have indicated that oxidative stress is involved in the aging process. D-Galactose (D-gal) is a reducing sugar that is normally present in the body and can be converted into aldose and hydroperoxide by galactose oxidase at high concentrations, resulting in the generation of oxygen-derived free radicals, which can also react with the amino groups present in proteins and peptides to form AGEs, leading to the production of ROS.[20] The liver and kidney are highly specialized organs involved in D-gal metabolism, and D-gal

exposure increases the production of intracellular reactive oxygen species (ROS) and lipid peroxidation in the liver and kidney.[9,10] Hence, administration of D-gal (150 mg kg^{-1} body weight, SI) to mice for 8 weeks has been widely used in antiaging and organ injury research to explore the underlying mechanisms in antioxidative pharmacology research.[21]

To date, natural metabolically active products have been widely tested as important sources for drug discovery in antiaging and aging-related diseases. Urolithin A is a major metabolite produced by rats and humans after the consumption of pomegranate juice or pure ellagitannin geraniin. Previous studies have shown that urolithin A has antioxidant and anti-inflammatory effects.[22] In the present study, we established a liver and kidney injury model through the subcutaneous administration of D-gal to explore the underlying mechanisms of urolithin A protection against D-gal-induced liver and kidney damage. To our knowledge, this study provided evidence for the first time that: (1) urolithin A possess excellent antioxidant activity *in vitro* antioxidant systems and (2) urolithin A treatment could protect mice against D-gal-induced oxidative liver and kidney damage in an aging model. Moreover, the protective effects of urolithin A are closely correlated to its antioxidative, anti-inflammatory and antiapoptotic properties.

It has been demonstrated that antioxidant enzymes can protect cellular compounds against damage induced by free radicals.[23] SOD, GSH-Px, CAT and T-AOC are important antioxidant enzymes. Under oxidative stress conditions, SOD is the first gatekeeper in the antioxidant defense system and it can catalyze the reduction of O_2^- to H_2O_2, the latter of which is further scavenged by catalysis from CAT and GSH-Px, resulting in the production of water and oxygen.[24,25] T-AOC represents a comprehensive antioxidant enzyme in the body; MDA, which is a lipid oxidation final product, is commonly used as a biomarker of oxidative stress.[26] Many studies have shown that oxidative stress is one of the key factors responsible for kidney aging, as revealed by the increasing levels of MDA and the decreasing activities of SOD, GSH-Px, CAT and T-AOC.[27] In accordance with previous reports, decreases in the activities of SOD, GSH-Px, CAT, and T-AOC, as well as increased MDA caused by D-gal, were observed in the present research, and our results showed that urolithin A treatment could obviously attenuate the activities of these antioxidant enzymes and the MDA levels in mouse livers and kidneys, which may be one mechanism by which urolithin A improves liver and kidney functions in D-gal-induced aging mice. These data suggested that urolithin A had an anti-aging effect and could protect the liver and kidney tissues of mice against D-gal-induced oxidative damage.

Inflammation is one of the leading causes of the many pathological states associated with oxidative stress.[28] It has been reported that proinflammatory cytokines, such as TNF-α, IL-1β and IL-6, are small secreted proteins that mediate and regulate inflammation. TNF-α is a key mediator in an inflammatory reaction that induces the innate immune response by stimulating the release of other inflammatory cytokines.[29] Moreover, TNF-α induces a number of physiological effects, including inflammation, septic shock, and cytotoxicity.[30] IL-1β has a wide range of immunomodulatory effects and may mediate inflammation or be directly involved in the inflammatory process.[31] IL-6 is a pivotal pro-inflammatory cytokine that is synthesized primarily by macrophages and can facilitate autoimmune phenomena, amplify acute inflammation and promote the evolution into a chronic inflammatory state. IL-6 plays a pivotal role in the acute phase response and multiple immunomodulatory functions. Here, we evaluated whether urolithin A regulates TNF-α, IL-1β and IL-6 expression in the livers and kidneys of D-gal-injured mice. Interestingly, urolithin A could markedly downregulate the expression levels of these multifunctional cytokines in the livers and kidneys of D-gal-treated mice, which suggests that urolithin A could attenuate the inflammatory injury induced by D-gal.

Moreover, histopathological changes in the liver and the activities of some serum enzymes, which are useful biomarkers of liver injury, were also evaluated in this study. Our results suggest that D-gal injection results in conspicuously elevated ALT and AST levels, hepatocyte apoptosis and inflammatory cell infiltration into hepatic tissue. However, these histopathological changes and increased levels of serum enzymes were ameliorated after long-term intervention with urolithin A, signifying that urolithin A had protective effects on D-gal-induced hepatic dysfunction *in vivo* during the experimental period.[32] BUN and Cr are two common renal function markers that increase in expression level with damage. In this study, it was observed that there were significant differences between the control and D-gal-induced aging mice with regards to the two renal damage markers, which was consistent with previous studies, thereby indicating that chronic administration of D-gal impaired the renal functions of mice. After inducing renal damage and treating mice with urolithin A for 8 weeks, the BUN and Cr levels were reduced, indicating that urolithin A could reverse the renal injury induced by D-gal in mice.[33] Multiple lines of evidence have shown that D-gal injection can cause kidney dysfunction as well as changes in kidney morphology. Decreased glomeruli, increased sclerosing glomeruli and diameter, and expanded renal capsules were observed in D-gal-induced aging mice; in contrast, these histopathological changes were notably ameliorated after long-term treatment with urolithin A, suggesting that administration of urolithin A has a protective effect on D-gal-damaged kidney tissues in mice.

It has been confirmed that the D-gal-induced aging process in mice is related to apoptosis, so we analyzed the protein levels of cleaved caspase-3, Bax and Bcl-2 by western blotting.[34,35] The Bcl-2 protein is a key factor in the inhibition of apoptosis; it is a known factor in cell aging, and its overexpression can effectively prevent the apoptosis induced by hydrogen peroxide, free radicals and microbial contamination.[36] On the other hand, the main function of Bax is to accelerate apoptosis and, together with Bcl-2, regulate cell apoptosis. However, the core molecule in apoptosis is cleaved caspase-3 (a cysteine protease), which is known to be mainly in charge of the execution of apoptosis.[10,37] It has commonly been believed that Bax acts downstream of cleaved caspase-3 activation, and thus, apoptosis is inhibited by the downregulation of cleaved caspase-3, which plays an irreplaceable role in apoptosis.[38] Our results showed that urolithin A intervention significantly downregulated Bcl-2 and Bax

protein expression and upregulated the expression of cleaved caspase-3. These data suggested that urolithin A treatment exerted an antiapoptotic effect in D-gal-induced liver and kidney injury by reducing the Bax/Bcl-2 ratio, which is viewed as a key indicator of cell survival and the inhibition of the activation of cleaved caspase-3.[39,40] However, the above all about anti-apoptotic effect of urolithin A may need to be further analyzed and confirmed due to lacking of total/uncleaved caspase-3 results (a key factor of apoptosis in mammals), which was a limitation for our study.

Conclusion

The present work demonstrates the improvement of urolithin A on liver and kidney dysfunction and histopathologic changes in D-gal-induced aging mice from the *in vivo* experimental results. The mechanism may be through enhancing the liver and kidney antioxidant capacity and attenuating the inflammatory response and apoptosis. Thus, urolithin A might have potential for further development into a promising pharmaceutical candidate for the treatment of age associated diseases.

Conflicts of interest

There are no conflicts to declare.

Acknowledgements

This work was supported by grants from the National Natural Science Foundation of China (31770381).

References

1 E. M. Fivenson, S. Lautrup, N. Sun, M. Scheibye-Knudsen, T. Stevnsner, H. Nilsen, V. A. Bohr and E. F. Fang, *Neurochem. Int.*, 2017, **3**, 202–209.
2 J. Fan, X. Yang, J. Li, Z. Shu, J. Dai, X. Liu, B. Li, S. Jia, X. Kou, Y. Yang and N. Chen, *Oncotarget*, 2017, **8**, 17475–17490.
3 Z. Dong, M. Xu, J. Huang, L. Chen, J. Xia, X. Chen, R. Jiang, L. Wang and Y. Wang, *Exp. Ther. Med.*, 2017, **14**, 616–622.
4 X. Chen, Y. Li, W. Chen, Z. Nong, J. Huang and C. Chen, *Neurochem. Res.*, 2016, **41**, 1–10.
5 M. Ghosh, J. Das and P. C. Sil, *Free Radical Res.*, 2012, **46**, 116–132.
6 M. Y. Xia, X. Y. Zhao, Q. L. Huang, H. Y. Sun, C. Sun, J. Yuan, C. He, Y. Sun, X. Huang, W. Kong and W. J. Kong, *FEBS Open Bio*, 2017, **7**, 759–776.
7 Z. Hong, Q. Zhuo, J. Zhang, B. Jiang, C. Liu and W. Gao, *RSC Adv.*, 2018, **8**, 10163–10171.
8 J. Gao, R. Zhou, X. You, F. Luo, H. He, X. Chang, L. Zhu, X. Ding and T. Yan, *Metab. Brain Dis.*, 2016, **31**, 771–778.
9 Z. Qu, J. Zhang, H. Yang, L. Huo, J. Gao, H. Chen and W. Gao, *Physiol. Behav.*, 2016, **154**, 114–125.
10 Y. Liu, L. Zhu, S. Liang, S. Yao, R. Li, S. Liu, Y. Ma, X. Zhou, J. Zhang, H. Zeng and X. Wang, *Lab. Invest.*, 2015, **95**, 504–514.
11 L. Tang, Y. Mo, Y. Li, Y. Zhong, S. He, Y. Zhang, Y. Tang, S. Fu, X. Wang and A. Chen, *Biochem. Biophys. Res. Commun.*, 2017, **486**, 774–780.
12 A. González-Sarrías, J. Tomé-Carneiro, A. Bellesia, F. A. Tomás-Barberán and J. C. Espín, *Food Funct.*, 2015, **6**, 1460–1469.
13 Y. Wang, Z. Qiu, B. Zhou, C. Liu, J. Ruan, Q. Yan, J. Liao and F. Zhu, *Toxicol. In Vitro*, 2015, **29**, 1107–1115.
14 M. Savi, L. Bocchi, P. Mena, M. Dall'Asta, A. Crozier, F. Brighenti, D. Stilli and D. Del Rio, *Cardiovasc. Diabetol.*, 2017, **16**, 80–92.
15 D. Ryu, L. Mouchiroud, P. A. Andreux, E. Katsyuba, N. Moullan, A. A. Nicolet-Dit-Félix, E. G. Williams, P. Jha, G. Lo Sasso, D. Huzard, P. Aebischer, C. Sandi, C. Rinsch and J. Auwerx, *Nat. Med.*, 2016, **22**, 879–888.
16 S. T. Wang, W. C. Chang, C. Hsu and N. W. Su, *J. Agric. Food Chem.*, 2017, **65**, 6870–6876.
17 E. Kaviani, M. Rahmani, A. Kaeidi, A. Shamsizadeh, M. Allahtavakoli, N. Mozafari and I. Fatemi, *Behav. Brain Res.*, 2018, **21**, 19–25.
18 D. D. Duan, K. X. Wang, Y. Z. Zhou, X. M. Qin, L. Gao and G. H. Du, *Rejuvenation Res.*, 2017, **20**, 506–516.
19 Y. Y. Wang, B. Z. Diao, L. H. Zhong, B. L. Lu, Y. Cheng, L. Yu and L. Y. Zhu, *Microb. Pathog.*, 2018, **119**, 49–53.
20 C. Liu, J. Hu, Z. Mao, H. Kang, H. Liu, W. Fu, Y. Lv and F. Zhou, *Clin. Interventions Aging*, 2017, **12**, 593–602.
21 Y. Zhuang, Q. Ma, Y. Guo and L. Sun, *Food Chem. Toxicol.*, 2017, **108**, 554–562.
22 C. M. Liu, J. Q. Ma and Y. Lou, *Food Chem. Toxicol.*, 2010, **48**, 2809–2817.
23 Q. Ruan, F. Liu, Z. Gao, D. Kong, X. Hu, D. Shi, Z. Bao and Z. Yu, *Mech. Ageing Dev.*, 2013, **134**, 89–97.
24 G. Karaolanis, A. Katsaros, V. V. Palla, S. Lionaki, D. Moris, E. Karanikola, M. Kravaritou, V. Drossos, T. Psarros, K. Triantafillou, N. Aleksandropoulos and G. Zografos, *Hellenic J. Cardiol.*, 2015, **56**, 160–168.
25 E. B. Kalaz, J. Çoban, A. F. Aydın, I. Doğan-Ekici, S. Doğru-Abbasoğlu, S. Öztezcan and M. Uysal, *J. Physiol. Biochem.*, 2014, **70**, 15–25.
26 Y. Zhang, L. H. Zhang, X. Chen, N. Zhang and G. Li, *Food Funct.*, 2018, **9**, 371–378.
27 J. M. Yuan, S. G. Carmella, R. Wang, Y. T. Tan, J. Adams-Haduch, Y. T. Gao and S. S. Hecht, *Carcinogenesis*, 2018, **39**, 948–954.
28 R. Charrad, A. Berraïes, B. Hamdi, J. Ammar, K. Hamzaoui and A. Hamzaoui, *Immunobiology*, 2016, **221**, 182–187.
29 N. Kurosawa, K. Shimizu and K. Seki, *Psychopharmacology*, 2016, **233**, 1725–1737.
30 U. Hoda, N. B. Agarwal, D. Vohora, S. Parvez and S. Raisuddin, *Nutr. Neurosci.*, 2016, **20**, 497–504.
31 A. Wytrykowska, M. Prosba-Mackiewicz and W. M. Nyka, *J. Oral Sci.*, 2016, **58**, 509–513.
32 A. Ahangarpour, S. A. Najimi and Y. Farbood, *J. Chin. Med. Assoc.*, 2016, **79**, 589–596.
33 Y. Feng, Y. H. Yu, S. T. Wang, J. Ren, D. Camer, Y. Z. Hua, Q. Zhang, J. Huang, D. L. Xue, X. F. Zhang, X. F. Huang and Y. Liu, *Pharm. Biol.*, 2016, **54**, 1027–1034.

34 D. Zhou, P. Liu, D. W. Sun, Z. J. Chen, J. Hu, S. M. Peng and Y. L. Liu, *Eur. Rev. Med. Pharmacol. Sci.*, 2017, **21**, 2785–2792.
35 H. M. Davis, R. Pacheco-Costa, E. G. Atkinson, L. R. Brun, A. R. Gortazar, J. Harris, M. Hiasa, S. A. Bolarinwa, T. Yoneda, M. Ivan, A. Bruzzaniti, T. Bellido and L. I. Plotkin, *Aging Cell*, 2017, **16**, 551–563.
36 Y. Xiong, G. Yepuri, S. Necetin, J. P. Montani, X. F. Ming and Z. Yang, *Diabetes*, 2017, **66**, 1636–1649.
37 A. P. Ryzhak, N. I. Chalisova, N. S. Lin'Kova, T. E. Nichik, A. V. Dudkov, N. V. Kolchina, G. A. Ryzhak and R. I. Khalimov, *Bull. Exp. Biol. Med.*, 2017, **162**, 534–538.
38 A. Mohankumar, G. Shanmugam, D. Kalaiselvi, C. Levenson, S. Nivitha, G. Thiruppathi and P. Sundararaj, *RSC Adv.*, 2018, **8**, 33753–33774.
39 X. J. Mi, J. G. Hou, S. Jiang, Z. Liu, S. Tang, X. X. Liu, Y. P. Wang, C. Chen, Z. Wang and W. Li, *J. Agric. Food Chem.*, 2019, **67**, 1392–1401.
40 Y. Mejíaspeña, B. Estébanez, P. Rodriguezmiguelez, R. Fernandez-Gonzalo, M. Almar, J. A. de Paz, J. González-Gallego and M. J. Cuevas, *Aging*, 2017, **9**, 408–418.

